Desalination and Water Treatment
www.deswater.com

doi: 10.5004/dwt.2023.29335

286 (2023) 197–204
February

Enhanced photocatalytic degradation performance of Bi_2WO_6 via O_3 modification

Wei Wu[a], Jianhua Ge[a,b,*], Baiqing Xiao[a,*], Zhou Wei[a], Wan Zhang[a], Xuyang Zheng[a]

[a]*School of Earth and Environment, Anhui University of Science and Technology, Huainan 232001, China, email: gejianhua13@163.com (J. Ge)*
[b]*Institute of Energy, Hefei Comprehensive National Science Center, Anhui, Hefei 230031, China*

Received 18 October 2022; Accepted 19 January 2023

ABSTRACT

Bi_2WO_6 with enhanced photocatlytic degradation performance was successfully synthesized by a facile O_3 etching method. The photocatalysts were characterized by X-ray diffraction, scanning electron microscopy, and ultraviolet-visible diffuse reflectance spectra. Characterization results revealed that the O_3 treated Bi_2WO_6 photocatalyst has abundant of oxygen vacancies, which could effectively restrain recombination of photon-generated carriers, broaden light absorption region, serve as photocatalytic reaction center. Moreover, the photocatalytic activities of the prepared photocatalysts were evaluated by the photocatalytic degradation of benzidine under a xenon lamp irradiation. The photocatalytic activity of treated Bi_2WO_6 photocatalyst samples with O_3 pose a greater improvement. Among that, the O_3-Bi_2WO_6-3-4 modifying with ozone flux of 3.0 L/min for 4 h photocatalytic degradation of benzidine wastewater reached ~76.0% in 180 min under the irradiation of xenon lamp light (λ = 420 nm), which is about ~2.1 times higher than that of pure Bi_2WO_6. Moreover, the photocatalytic activities of the modified Bi_2WO_6 via O_3 exhibit without significantly decrease after four cycles, indicating that the photocatalyst has a favourable application prospect.

Keywords: Bi_2WO_6; Benzidine; Ozone modification; Degradation

1. Introduction

It is well-known that photocatalytic process is an environmental technology in hydrogen generation, contaminant degradation, nitrogen photofixation, and so on recently [1–5]. Studies have revealed that photocatalyst is crucial to photocatalytic technology. Since then, a large number of photocatalysts have been developed successively by researchers in recent years [6–13]. Among those photocatalysts, Bi_2WO_6 is a kind of Aurivillius type oxide, which has been paid much attention for its high specific surface area, higher light absorption capacity, and so on [14]. For instance, as early as in 1999, Kudo successfully fabricated Bi_2WO_6 through solid phase method for the first time, which possesses favorable photocatalytic activity under visible light irradiation [15]. However, the narrow absorption range and low migration rate of photo-generated charges of Bi_2WO_6, which restrict the performance of photocatalytic degradation of pollutants [16]. Since then, with an aim to overcome the drawbacks of Bi_2WO_6, more and more scientific literatures have been published about the modification of Bi_2WO_6, such as morphology control, elements doping, construction of hetero-junction structure [17–28]. For example, $BiPO_4$/Bi_2WO_6 heterojunction photocatalyst was synthesized, which could absorb sunlight efficient for photocatalytic degradation of organic contaminants [29].

As is well known, O_3 is an oxidative and corrosive gas, which is used as a deodorizer, bleaching agent, and a disinfectant in the treatment of wastewater and drinking water [30]. Zhang et al. [31] reported a novel TiO_2 photocatalyst

* Corresponding authors.

via ozone modification method. Meanwhile, in order to improve the photocatalytic nitrogen fixation activity, our group synthesized g-C_3N_4 photocatalyst using ozone etching method, and we found that the ozone treated g-C_3N_4 has enhanced Brunauer–Emmett–Teller (BET) specific surface area, reduction property, and photo-induced charge migration efficiency [32].

In this study, the Bi_2WO_6 photocatalyst was firstly treated with O_3 etching method. The properties of the phtotocatalyst samples have been characterized via X-ray diffraction (XRD), scanning electron microscopy (SEM), and ultraviolet-visible (UV-Vis) analysis. Furthermore, the photocatalytic activities of the materials have been evaluated by degradation of benzidine wastewater in the photo degradation process, which is effective way to solve the environmental issue of the extensive use of benzidine.

2. Experimental set-up

2.1. Chemicals

All the chemicals (analytical grade), primarily including bismuth nitrate pentahydrate [($Bi(NO_3)_3{\cdot}5H_2O$, ≥99.0%)], potassium iodide (KI, ≥99.0%), sodium tungstate dihydrate ($Na_2WO_4{\cdot}2H_2O$, ≥99.5%), ethylene glycol ($C_2H_6O_2$, ≥98.0%), anhydrous ethanol (C_2H_6O, ≥95.0%), benzidine ($C_{12}H_{12}N_2$, ≥95.0%), isopropanol (C_3H_7OH, ≥98.0%), tert-butanol ($C_4H_{10}O$, ≥99.0%), were purchased from Shanghai Aladdin Biochemical Technology Co., Ltd., (China) and without further treatment.

2.2. Synthesis of the photocatalysts

2.2.1. Preparation of Bi_2WO_6

The Bi_2WO_6 photocatalyst was prepared as follows: A certain amount of $Bi(NO_3)_3{\cdot}5H_2O$ and $Na_2WO_4{\cdot}2H_2O$ were dissolved in 20 mL ethylene glycol, respectively. Subsequently, the above solutions were mixed together under magnetic stirring, and then, the mixed solution was transferred into 100 mL autoclave, heated at 160°C for 24 h. The resulting product was filtered, washed with deionized water, absolute ethanol several times, respectively, and dried in the air [33].

2.2.2. Fabrication of Bi_2WO_6 via O_3 modification

The ozone treated Bi_2WO_6 was obtained through O_3 etching method. In a typical synthesis, the Bi_2WO_6 suspended solutions were treated according to the ozone gas at rate of X L/min for Y hours, which was denoted as O_3-Bi_2WO_6-X-Y.

2.3. Characterization of photocatalysts

All the photocatalyst samples were determined using X-ray power diffraction (XRD, 5°/min, 10°~80° in 2θ, SmartLab SE, Japan), scanning electron microscopy (SEM, FlexSEM 1000, Hitachi, Japan), Fourier-transform infrared (FT-IR, Nicolet is50, China), and X-ray photoelectron spectroscopy (XPS, ESCALAB 250Xi, USA), Brunauer–Emmett–Teller (BET, ASAP2020, America). In addition, the optical and electronic properties were characterized on a UV-Visible spectrophotometry (UV-Vis, Lambda 950, PerkinElmer, America) and electrochemical impedance spectroscopy (EIS, CHI760E, Shanghai Chenghua Technology Co., Ltd., China).

2.4. Photocatalytic activity measurement

The photocatalytic activity of the as-synthesized samples was carried out in a slurry reactor containing benzidine solution (~200 mL, 5.0 mg/L). A Xe lamp was used as a sunlight source. During given time intervals, ~8.0 mL suspension liquid were collected, centrifuged immediately, and the concentration of benzidine after illumination was determined by checking the absorbance at ~553 nm adopting a UV-Vis spectrophotometer.

3. Results and discussion

3.1. XRD analysis

The phase compositions of the as-synthesized samples were analyzed by XRD. As depicted in Fig. 1, the diffraction peaks of Bi_2WO_6 are consistent with the standard card of rhombic Bi_2WO_6 (PDF No.39-0256) [34]. Meanwhile, there is no significant change in the phase compositions of Bi_2WO_6 via ozone modification. It's an interesting phenomenon that the intensity of the diffraction peaks of the Bi_2WO_6 photocatalysts at the (131), (200), (202), and (331) crystal planes are comparatively reduced after ozone etching process, suggesting that the effects of O_3 etching can inhibit the growth of corresponding crystal face.

3.2. SEM analysis

The surface morphology of the ozone treated Bi_2WO_6 and pure Bi_2WO_6 photocatalyst samples were investigated by SEM. As Fig. 2 depicts, it could clearly demonstrate that the morphologies of the photocatalysts are sphere with hierarchical microstructure, which is consists of a large quantity of Bi_2WO_6 nanosheets, and no other morphologies were observed. After ozone modification is introduced, the morphologies of the Bi_2WO_6 almost remains unchanged.

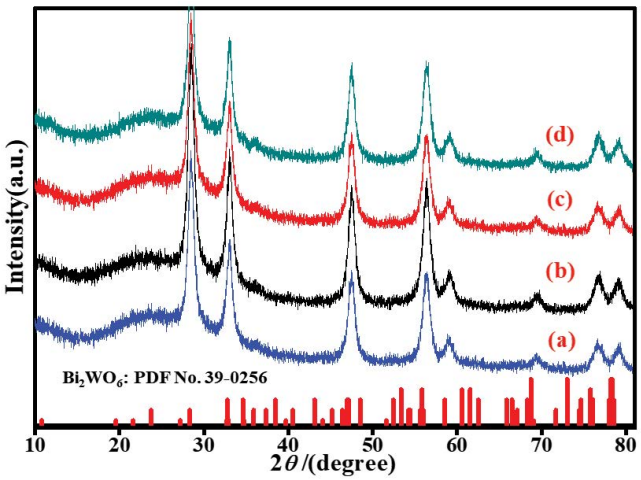

Fig. 1. X-ray diffraction patterns of the photocatalysts' modified and unmodified Bi_2WO_6. (a) Pure Bi_2WO_6, (b) O_3-Bi_2WO_6-2-4, (c) O_3-Bi_2WO_6-3-1, and (d) O_3-Bi_2WO_6-3-4.

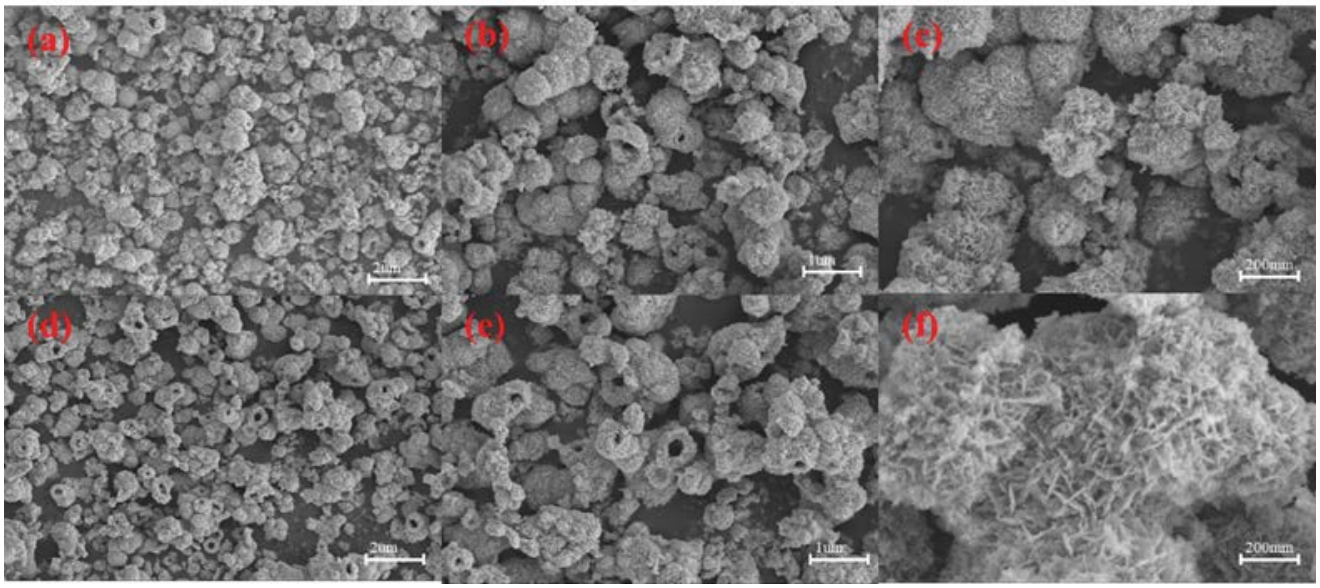

Fig. 2. Scanning electron microscopy images of the modified and unmodified Bi_2WO_6 samples. (a–c) Pure Bi_2WO_6 and (d–f) O_3-Bi_2WO_6-3-4.

3.3. XPS analysis

With an aim to determine the surface properties of samples, XPS was used to characterize the chemical composition of the ozone treated Bi_2WO_6 and pure Bi_2WO_6. The survey XPS spectrum in Fig. 3a clearly reveals the existence of Bi, O and W element. Among them, the oxygen peak at ~530.2 eV can be attributed to the lattice oxygen of photocatalyst, and from the absorbed O_2 and H_2O on the surface. Compared with Bi_2WO_6, the binding energy of O 1s at ~534.1 eV, manifesting the existence of abundant oxygen vacancies (OVs) [35] (Table 1). Furthermore, the obtained W/O mass ratio of samples were ca.~6.39, ~9.15, respectively, suggesting the oxygen vacancies are formed in photocatalyst via ozone modification. Meanwhile, it can be observed that two strong peaks with binding energy of ~159.3 and ~164.65 eV, assigned to Bi $4f_{5/2}$ and Bi $4f_{7/2}$, respectively. The high-resolution of W 4f at ~36.0 and ~38.0 eV, corresponding to W $4f_{7/2}$ and W $4f_{5/2}$ peaks, respectively [36–38].

3.4. FT-IR analysis

In order to identify the changes in the functional groups of the Bi_2WO_6 via O_3 modification, the as-prepared samples were further monitored by FT-IR spectroscopy. As shown in Fig. 4, the two characteristic peaks at ~3,428 and ~1,369 cm^{-1} are ascribed to the bending vibration of O–H, respectively. While the characteristic peaks at ~820, ~730 and ~568 cm^{-1} are ascribed to the stretching of W–O–W, W–O and BI–O, it indicates that the structure of Bi_2WO_6 has not been changed via O_3 modification.

3.5. UV-Vis analysis

The UV-Vis diffuse reflectance spectra and band gap of Bi_2WO_6 and O_3-Bi_2WO_6-3-4 composite are displayed in Fig. 5. It can be seen that the Bi_2WO_6 and O_3-Bi_2WO_6-3-4 samples have an intense adsorption within the range of 400–800 nm. Meanwhile, the absorption ability of the ozone treated Bi_2WO_6 is enhanced, so it can be inferred that the oxygen vacancies exist in O_3-Bi_2WO_6-3-4, thus altering its optical properties. In addition, the band gaps of the as-prepared photocatalysts were calculated using the Kubelka–Munk equation. It is found that the gaps of Bi_2WO_6 and O_3-Bi_2WO_6-3-4 is ~3.06 and ~3.07 eV, respectively.

3.6. BET analysis

N_2 adsorption–desorption experiments were employed to determine the specific surface area and pore size of the as-prepared photocatalysts. Fig. 6 reveals the N_2 absorption–sorption isotherms of Bi_2WO_6 and O_3-Bi_2WO_6-3-4, which belong to type III according to the IUPAC classification, demonstrating the presence of mesopores in the samples [39]. As shown in Table 2, the surface area of Bi_2WO_6 has almost no change via ozone etching. In addition, the smaller pore volume and pore diameter of O_3-Bi_2WO_6-3-4 is can adsorb easily benzidine molecules, thus enhanced the degradation performance of benzidine.

3.7. Photoelectric property analysis

With an aim to monitor the photoelectric property of as-prepared photocatalyst, the transient photocurrent and EIS were obtained using electrochemical workstation. As shown in Fig. 7a, the O_3-Bi_2WO_6-3-4 displays approximately 1.3 times higher photocurrent intensity than pure Bi_2WO_6, suggesting that the O_3-Bi_2WO_6-3-4 photocatalyst probably present more separation efficiency of photogenerated carriers in the photocatalytic reaction system under light irradiation. Hence, the higher photocurrent density is attributed to the separation of photoinduced carriers in the photocatalyst [40]. Furthermore, the EIS of Bi_2WO_6 and O_3-Bi_2WO_6-3-4

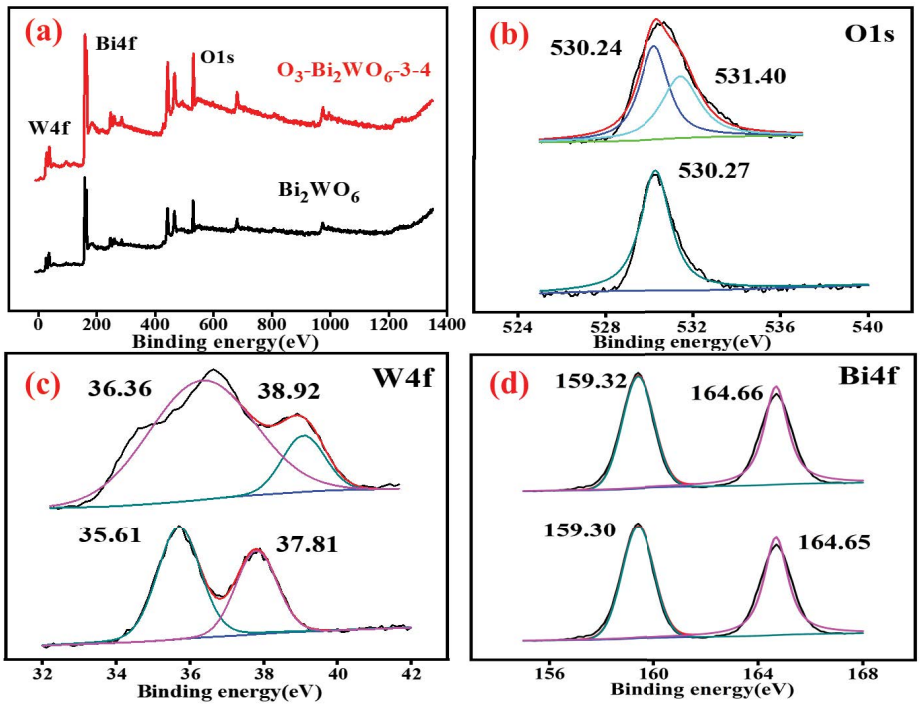

Fig. 3. X-ray photoelectron spectroscopy diagram of the modified and unmodified Bi_2WO_6 samples. (a) Bi_2WO_6 and O_3-Bi_2WO_6-3-4, (b) O 1s of Bi_2WO_6 and O_3-Bi_2WO_6-3-4, (c) W 4f of Bi_2WO_6 and O_3-Bi_2WO_6-3-4, and (d) Bi 4f of Bi_2WO_6 and O_3-Bi_2WO_6-3-4.

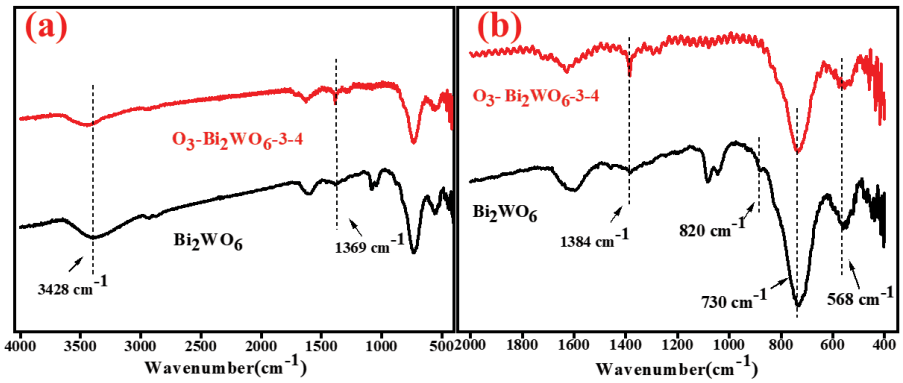

Fig. 4. Fourier-transform infrared spectra of pure Bi_2WO_6 and O_3-Bi_2WO_6-3-4.

samples were measured. The impedance curve radius of Bi_2WO_6 is larger than that of O_3-Bi_2WO_6-3-4, indicating that O_3-Bi_2WO_6-3-4 sample has more effective photoinduced charge separation properties at the interface of photocatalyst [41].

3.8. Photocatalytic performance of photocatalyst

3.8.1. Effect of O_3 modification time

Fig. 8a shows that degradation rate of benzidine by pure Bi_2WO_6 was 31.5%. O_3 promoted photocatalytic activity of the Bi_2WO_6 before 5 h of modification (degradation rate was 73.8%), but treatment of O_3 for too long may inhibit its degradation performance, and the degradation rate decreases to 64.8% at 5 h. With Electrochemical performance analysis (Fig. 7), O_3 modification made the Bi_2WO_6 photocurrent intensity increase, which benefits oxygen vacancies to promote photogenerated carrier separation and strengthened the photocatalytic activity of the Bi_2WO_6.

3.8.2. Effect of O_3 flux

The degradation rate of Bi_2WO_6 treated with O_3 for 4 h reached the highest 53% at 3.0 L/min (Fig. 6b), comparing with pure Bi_2WO_6, the degradation efficiency was nearly doubled. It is worth mentioning that the degradation efficiency of Bi_2WO_6 treated under the flux of 1.5, 2.0, and 4.0 L/min ozone is improved to a certain extent, and the degradation rates were 48.2%, 43.8% and 36.5%, respectively.

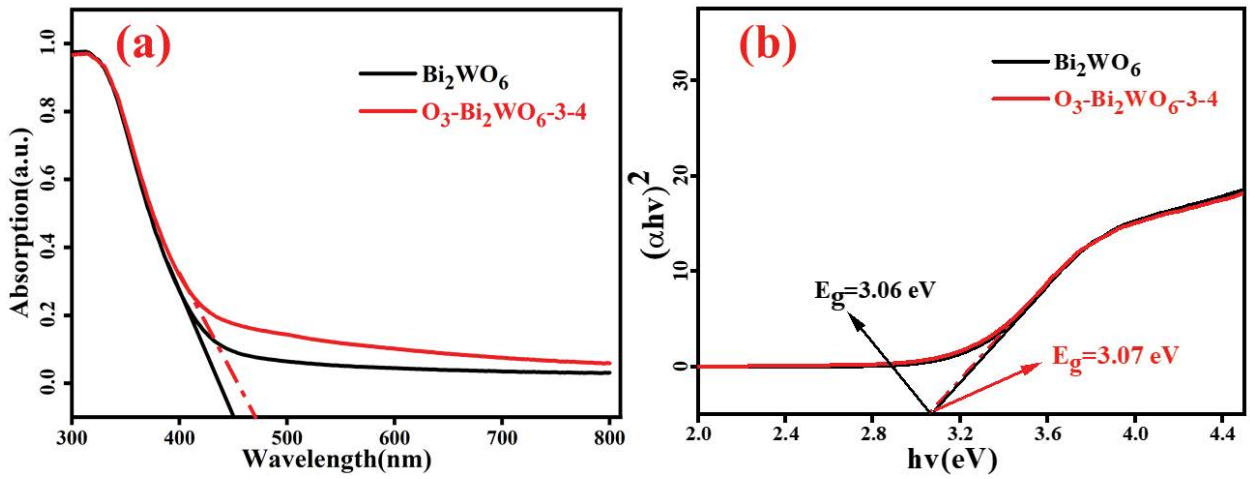

Fig. 5. UV-Vis diffuse reflection absorption spectrum of Bi_2WO_6 and O_3-Bi_2WO_6-3-4.

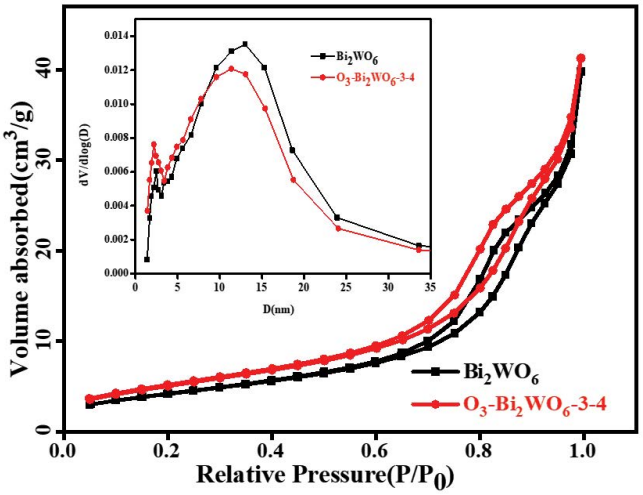

Fig. 6. Nitrogen adsorption–desorption isotherm and corresponding pore-size distribution curves of Bi_2WO_6 and O_3-Bi_2WO_6-3-4.

Table 1
Bi, W and O peak areas of Bi_2WO_6 and O_3-Bi_2WO_6-3-4

Area	Bi	W	O	W:Bi:O
O_3-Bi_2WO_6-3-4	170,031.0	38,437.5	350,391.1	1:7.12:6.39
Bi_2WO_6	169,192.8	23,748.4	151,974.1	1:4.42:9.15

Table 2
Physical properties of Bi_2WO_6 and O_3-Bi_2WO_6-3-4 samples and their voids

Samples	Surface area (m^2/g)	Pore diameter (nm)	Pore volume (cm^3/g)
Bi_2WO_6	81.1	13	0.331
O_3-Bi_2WO_6-3-4	81.3	11.385	0.284

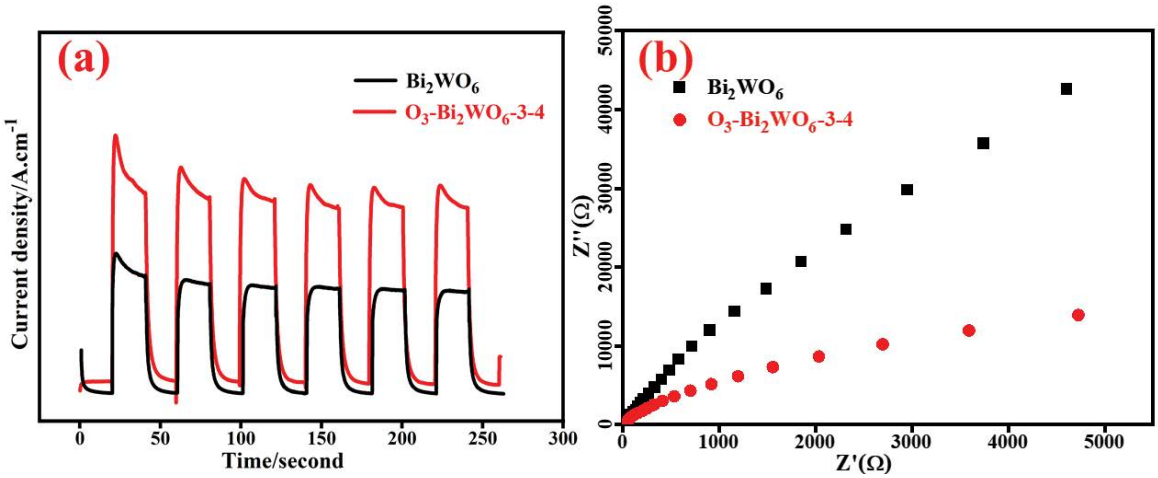

Fig. 7. Electrochemical performance analysis of Bi_2WO_6 and O_3-Bi_2WO_6-3-4.

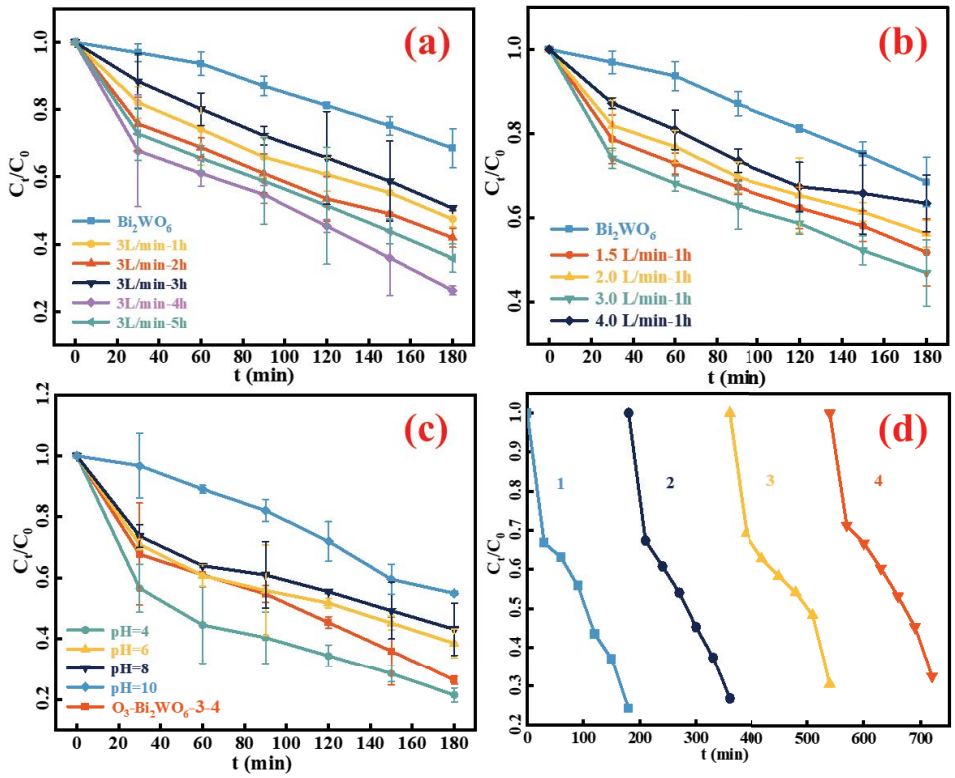

Fig. 8. The influence of: (a) ozone modification time (dose = 0.2 g; volume = 200 mL; concentration = 5.0 mg/L; flux = 3.0 L/min; pH = 7.0), (b) ozone flux (dose = 0.2 g; volume = 200 mL; concentration = 5.0 mg/L; t = 4 h; pH = 7.0), (c) pH (dose = 0.2 g; volume = 200 mL; concentration = 5.0 mg/L; flux = 3.0 L/min; t = 4 h) and (d) O_3-Bi_2WO_6-3-4 repeated use experiments (dose = 0.2 g; volume = 250 mL; concentration = 5.0 mg/L; pH = 7.0).

Table 3
Comparison of photocatalytic efficiency obtained in this work to other textile wastewater degradation studies[a]

Pollutant	Photocatalyst	Dye conc. (mg/L)	Dye volume (mL)	Doping materials	Optimum doping	pH	Irrad. time (min)	Eff. %	References
Methyl orange dye	CQD/TiO_2	20	20	CQD	1:10	11	180	71.9	[42]
Textile wastewater	TiO_2-Anthill clay	3.01	50	Anthill clay	2:3	2	60	70.92	[43]
Methylene blue	ZnO/ZTO	3.12	nr	ZnO	1:15	8.37	180	94	[44]
Methylene blue	$Ca_{10}(PO_4)_6(OH)_2$	5	150	nr	nr	nr	360	54	[45]
Congo red	CdS/g-C_3N_4	25	50	CdS	1:1	7	10	100	[46]
Methylene blue	Al-F/TiO_2	4	10	Al, F	1:2:10	nr	120	83	[47]
Methyl orange dye	Ag/ZnO	15	nr	Ag	1:100	11	180	84.67	[48]

[a]This table is indicative and any comparisons are subject to additional variables such as the catalyst surface area and initial pH of the solution.
Note: nr: not reported.

3.8.3. Effect of solution pH

The pH of the dye solution is an important factor in the photocatalytic process. To study the impact of the pH on photodegradation efficiency, experiments were carried out in pH ranges of 4.0–10.0, at fixed initial dye concentration (5.0 mg/L), and photocatalyst dose (0.20 g O_3-Bi_2WO_6-3-4) for 180 min Xe irradiation. It was observed that the increase of pH from 4.0 to 10.0, decreases the photodegradation efficiency (from 78.6% to 45.0%). The experimental results showed that higher degradation efficiency was found in the acidic medium alkaline medium than in the neutral and alkaline medium. This was formed due to the acidic solution provides a large amount of h^+ to participate in the reaction as the active group in the solution.

3.8.4. Reusability of the O_3-Bi_2WO_6-3-4 photocatalyst

The result of the catalyst reusability and stability studies is presented in Fig. 8d. The photocatalytic degradation process was conducted under the optimum conditions of O_3 modification time of 4 h, O_3 flux of 3.0 L/min and dye

solution pH of 4.0. The photocatalyst was reused for four reaction cycles, and the dye removal efficiencies for the cycles were obtained to be 75.8%, 73.1%, 69.2%, and 67.2%, respectively. It was observed that the benzidine removal efficiency declines insignificantly as the reaction cycle proceeds, indicating that the prepared O_3-Bi_2WO_6-3-4 catalyst has a stable degradation effect.

4. Conclusions

The main objective of this work is to investigate the effect of ozone on photocatalytic performance of Bi_2WO_6 and its mechanism. In conclusion, compared with pure Bi_2WO_6, the O_3 treated Bi_2WO_6 with abundant of oxygen vacancies could effectively restrain the recombination of photon-generated carriers and enhance photocatalytic degradation properties. The optimized values for ozone flux, treated time, and pH, were 3.0 L/min, 4 h, 4.0, respectively. At these conditions, the removal percentage for benzidine wastewater was predicted to be 73.8%, which is about ~2.1 times higher than that of pure Bi_2WO_6. Compared with other pure phase or other modified photocatalysts, O_3-Bi_2WO_6-3-4 showed considerable degradation capacity (Table 3).

In practice, more work is required toward establishing Bi_2WO_6 as an effective photocatalytic for a wide range of textile wastewaters. Real textile wastewaters often contain several dyes, some of these may compete with benzidine. This would result in lower removal efficiency for benzidine and an overall decreased performance for the photocatalytic.

Acknowledgments

This work was partly financial supported by the Institute of Energy, Hefei Comprehensive National Science Center under Grant No. 21KZS217, Anhui Province Engineering Laboratory of Water and Soil Resources Comprehensive Utilization and Ecological Protection in High Groundwater Mining Area (No. 2022-WSREPMA-03), and Anhui Province University Outstanding Young Talents Project (Grants No. gxyq2020012), Natural Science Fund of Anhui Province (Grants No. 1808085ME139), University Scientific Research Project of Anhui Provincial Educational Committee (No. KJ2020A0318).

References

[1] P. Raizada, S. Sharma, A. Kumar, P. Singh, A.A.P. Khan, A.M. Asiri, Performance improvement strategies of $CuWO_4$ photocatalyst for hydrogen generation and pollutant degradation, J. Environ. Chem. Eng., 8 (2020) 104230, doi: 10.1016/j.jece.2020.104230.

[2] S. Vignesh, S. Suganthi, J.K. Sundar, V. Raj, P.R.I. Devi, Highly efficient visible light photocatalytic and antibacterial performance of PVP capped Cd:Ag:ZnO photocatalyst nanocomposites, Appl. Surf. Sci., 479 (2019) 914–929.

[3] F. Shojaei, B. Mortazavi, X.Y. Zhuang, M. Azizi, Silicon diphosphide (SiP_2) and silicon diarsenide ($SiAs_2$): novel stable 2D semiconductors with high carrier mobilities, promising for water splitting photocatalysts, Mater Today Energy, 16 (2020) 100377, doi: 10.1016/j.mtener.2019.100377.

[4] T. Ishii, A. Anzai, A. Yamamoto, H. Yoshida, Calcium zirconate photocatalyst and silver cocatalyst for reduction of carbon dioxide with water, Appl. Catal., B, 277 (2020) 119192, doi: 10.1016/j.apcatb.2020.119192.

[5] H.A. Najafabadi, A.R. Fattahi, M. Asemi, G. Majid, Performance enhancement of dye-sensitized solar cells by plasma treatment of $BaSnO_3$ photoanode, J. Alloys Compd., 818 (2020) 152856, doi: 10.1016/j.jallcom.2019.152856.

[6] Y.G. Wang, Y.C. Wang, J. Bai, S.B. Duan, R.M. Wang, W.-M. Lau, *In-situ* etching synthesis of 3D self-supported serrated Ni-WO_3 for oxygen evolution reaction, J. Alloys Compd., 893 (2022) 162134, doi: 10.1016/j.jallcom.2021.162134.

[7] T. Sansenya, N. Masri, T. Chankhanittha, T. Senasu, J. Piriyanon, S. Mukdasai, S. Nanan, Hydrothermal synthesis of ZnO photocatalyst for detoxification of anionic azo dyes and antibiotic, J. Phys. Chem. Solids, 160 (2022) 110353, doi: 10.1016/j.jpcs.2021.110353.

[8] A.I. Ali, S. Moradi, S.R. Seyede, F. Ghanbari, E. Dehghanifard, B. Kakavandi, Peroxymonosulfate catalyzed by core/shell magnetic ZnO photocatalyst towards malathion degradation: enhancing synergy, catalytic performance and mechanism, Sep. Purif. Technol., 275 (2021) 119163, doi: 10.1016/j.seppur.2021.119163.

[9] A.M. Ali, M.A. Sayed, H. Algarni, V. Ganesh, M. Aslam, A.A. Ismail, M.H. El-Bery, Synthesis, characterization and photoelectric properties of Fe_2O_3 incorporated TiO_2 photocatalyst nanocomposites, Catalysts, 11 (2021) 1062, doi: 10.3390/catal11091062.

[10] C. Guo, L.Z. Chu, Q. Zhang, Z. Li, G.X. Yang, F. Peng, The zinc vacancy induced CdS/ZnS Z-scheme structure as a highly stable photocatalyst for hydrogen production, J. Alloys Compd., 888 (2021) 161620, doi: 10.1016/j.jallcom.2021.161620.

[11] T. Senasu, S. Nijpanich, S. Juabrum, N. Chanlek, S. Nanan, CdS/BiOBr heterojunction photocatalyst with high performance for solar-light-driven degradation of ciprofloxacin and norfloxacin antibiotics, Appl. Surf. Sci., 567 (2021) 150850, doi: 10.1016/j.apsusc.2021.150850.

[12] Y. Liu, B. Wei, L.L. Xu, H. Gao, M.Y. Zhang, Generation of oxygen vacancy and OH radicals: a comparative study of Bi_2WO_6 and Bi_2WO_{6-X} nanoplates, ChemCatChem, 7 (2015) 4076–4084.

[13] C.H. Lu, R.Y. Chen, X. Wu, M.F. Fan, Y.H. Liu, Z.G. Le, S.J. Jiang, S.Q. Song, Boron doped g-C_3N_4 with enhanced photocatalytic UO_2^{2+} reduction performance, Appl. Surf. Sci., 360 (2016) 1016–1022.

[14] Ph. Boullay, G. Trolliard, D. Mercurio, J.M. Perez-Mato, L. Elcoro, Toward a unified approach to the crystal chemistry of Aurivillius-Type compounds.: I. The structural model, J. Solid State Chem., 164 (2002) 252–260.

[15] K. Akihiko, H. Satoshi, H_2 or O_2 evolution from aqueous solutions on layered oxide photocatalysts consisting of Bi^{3+} with $6s^2$ configuration and d^0 transition metal ions, Chem. Lett., 28 (1999) 1103–1104.

[16] Z.Y. Jiang, X.Z. Liang, H.L. Zheng, Y.Y. Liu, Z.Y. Wang, P.G. Wang, X.Y. Zhang, X.Y. Qin, Y. Dai, B.B. Huang, Photocatalytic reduction of CO_2 to methanol by three-dimensional hollow structures of Bi_2WO_6 quantum dots, Appl. Catal., B, 219 (2017) 209–215.

[17] F.Y. Zhu, Y.Z. Lv, J.J. Li, J. Ding, X.H. Xia, L.L. Wei, J.Q. Jiang, G.S. Zhang, Q.L. Zhao, Enhanced visible light photocatalytic performance with metal-doped Bi_2WO_6 for typical fluoroquinolones degradation: efficiencies, pathways and mechanisms, Chemosphere, 252 (2020) 126577, doi: 10.1016/j.chemosphere.2020.126577.

[18] M. Shang, W.Z. Wang, L. Zhang, H.L. Xu, Bi_2WO_6 with significantly enhanced photocatalytic activities by nitrogen doping, Mater. Chem. Phys., 120 (2010) 155–159.

[19] J. Ren, W.Z. Wang, S.M. Sun, L. Zhang, J. Chang, Enhanced photocatalytic activity of Bi_2WO_6 loaded with Ag nanoparticles under visible light irradiation, Appl. Catal., B, 92 (2009) 50–55.

[20] S.S. Zhang, W.H. Pu, A.Y. Chen, Y.K. Xu, Y.Y. Wang, C.Z. Yang, J.Y. Gong, Oxygen vacancies enhanced photocatalytic activity towards VOCs oxidation over Pt deposited Bi_2WO_6 under visible light, J. Hazard. Mater., 384 (2020) 121478, doi: 10.1016/j.jhazmat.2019.121478.

[21] Y.C. Bai, T.Y. Wang, X.Y. Zhao, W. Mao, S.X. Liu, Synthesis of novel ternary Bi_2WO_6/CeO_2/g-C_3N_4 composites with enhanced visible light photocatalytic activity for removal of organic and

Cr(IV) from wastewater, J. Mater. Sci.: Mater. Electron., 31 (2020) 17524–17534.
[22] C. Cui, R.H. Guo, H.Y. Xiao, E. Ren, Q.S. Song, C. Xiang, X.X. Lai, J. Lana, S.X. Jiang, Bi_2WO_6/Nb_2CT_X mXene hybrid nanosheets with enhanced visible-light-driven photocatalytic activity for organic pollutants degradation, Appl. Surf. Sci., 505 (2020) 144595, doi: 10.1016/j.apsusc.2019.144595.
[23] Z.M. Qiang, X.M. Liu, F. Li, T.H. Li, M. Zhang, H. Singh, M. Huttula, W. Cao, Iodine doped Z-scheme $Bi_2O_2CO_3/Bi_2WO_6$ photocatalysts: facile synthesis, efficient visible light photocatalysis, and photocatalytic mechanism, Chem. Eng. J., 403 (2021) 126327 (1–42).
[24] M. Brigante, G. Zanini, M. Avena, Effect of humic acids on the adsorption of paraquat by goethite, J. Hazard. Mater., 184 (2010) 241–247.
[25] Y. Liu, B. Wei, L.L. Xu, H. Gao, M.Y. Zhang, Generation of oxygen vacancy and OH radicals: a comparative study of Bi_2WO_6 and Bi_2WO_{6-X} nanoplates, ChemCatChem, 7 (2016) 4076–4084.
[26] Y.L. Li, Y.M. Liu, J.S. Wang, E. Uchaker, Q.F. Zhang, S.B. Sun, Y.X. Huang, J.Y. Li, G.Z. Cao, Titanium alkoxide induced BiOBr-Bi_2WO_6 mesoporous nanosheet composites with much enhanced photocatalytic activity, J. Mater. Chem. A, 1 (2013) 7949–7956.
[27] W.H. Zhang, N. Yu, L.S. Zhang, K.W. Jiang, Y.Z. Chen, Z.G. Chen, Synthesis of Yb^{3+}/Er^{3+} CO-doped Bi_2WO_6 nanosheets with enhanced photocatalytic activity, Mater. Lett., 163 (2016) 16–19.
[28] Z.K. Cui, J.Q. Zhou, D.W. Zeng, From BiOCl to Bi_2WO_6 in Bi–W–Cl–O solvothermal system: phase-morphology evolution and photocatalytic performance, Mater. Technol., 30 (2014) 23–27.
[29] Y.Y. Zhu, Y.J. Wang, Q. Ling, Y.F. Zhu, Enhancement of full-spectrum photocatalytic activity over $BiPO_4/Bi_2WO_6$ clomposites, Appl. Catal., B, 200 (2017) 222–229.
[30] J. Tabla-Hernandez, A.G. Hernandez-Ramirez, E. Martinez-Tavera, P.F. Rodriguez-Espinosa, E. Mangas-Ramírez, Impacts on water quality by *in-situ* induced ozone-oxygen oxidation in a polluted urban reservoir, Sci. Total Environ., 735 (2020) 139364, doi: 10.1016/j.scitotenv.2020.139364.
[31] F. Zhang, B. Hong, W.S. Zhao, Y. Yang, J. Bao, C. Gao, S. Sun, Ozone modification as an efficient strategy for promoting the photocatalytic effect of TiO_2 for air purification, Chem. Commun., 55 (2019) 3757–3760.
[32] L. Zhang, J.H. Ge, Y.J. Liu, X.Y. Zheng, P.W. Du, Ozone modification as an efficient strategy for photocatalytic nitrogen fixation under visible light irradiation, J. Porous Mater., 28 (2021) 825–834.
[33] S.P. Hu, C.Y. Xu, Z. Liang, Solvothermal synthesis of Bi_2WO_6 hollow structures with excellent visible-light photocatalytic properties, Mater. Lett., 95 (2013) 117–120.
[34] A. Etogo, R. Liu, J.B. Ren, L.W. Qi, C.C. Zheng, J.Q. Ning, Y.J. Zhong, Y. Hu, Facile one-pot solvothermal preparation of Mo-doped Bi_2WO_6 biscuit-like microstructures for visible-light-driven photocatalytic water oxidation, J. Mater. Chem. A, 4 (2016) 13242–13250.
[35] L. Zhang, W.Z. Wang, D. Jiang, E. Gao, S.M. Sun, Photoreduction of CO_2 on BiOCl nanoplates with the assistance of photoinduced oxygen vacancies, Nano Res., 8 (2015) 821–831.
[36] Z. Nie, D.K. Ma, G.Y. Fang, W. Chen, S.M. Huang, Concave Bi_2WO_6 nanoplates with oxygen vacancies achieving enhanced electrocatalytic oxygen evolution in near-neutral water, J. Mater Chem. A, 4 (2015) 2438–2444.
[37] J.G. Wang, H. Liang, C. Zhang, B. Jin, Y. Men, Bi_2WO_{6-X} nanosheets with tunable Bi quantum dots and oxygen vacancies for photocatalytic selective oxidation of alcohols, Appl. Catal., B, 256 (2019) 117874, doi: 10.1016/j.apcatb.2019.117874.
[38] T.Y. Wang, J.Q. Liu, P.F. Wu, C.T. Feng, D.J. Wang, H.M. Hu, G.L. Xue, Direct utilization of air and water as feedstocks in the photo-driven nitrogen reduction reaction over a ternary Z-scheme SiW_9Co_3/PDA/BWO hetero-junction, J. Mater. Chem. A, 8 (2020) 16590–16598.
[39] R. Ahmad, R.S. Singh, B. Pal, A C_3N_4 surface passivated highly photoactive Au-TiO_2 tubular nanostructure for the efficient H_2 production from water under sunlight irradiation, Appl. Catal., B, 213 (2017) 9–17.
[40] H. Xu, J. Yan, Y.G. Xu, Y.H. Song, H.M. Li, J.X. Xia, C.J. Huang, Novel visible-light-driven AgX/graphite-like C_3N_4(X = Br, I) hybrid materials with synergistic photocatalytic activity, Appl. Catal., B, 129 (2013) 182–193.
[41] X.J. Bai, L. Wang, Y.F. Zhu, Visible photocatalytic activity enhancement of $ZnWO_4$ by graphene hybridization, ACS Catal., 2 (2012) 2769–2778.
[42] M. Shafique, M.S. Mahr, M. Yaseen, H.N. Bhatti, CQD/TiO_2 nanocomposite photocatalyst for efficient visible light-driven purification of wastewater containing Methyl orange dye, Mater. Chem. Phys., 278 (2022) 125583, doi: 10.1016/j.matchemphys.2021.125583.
[43] A.S. Yusuff, I.I. Olateju, O.A. Adesina, TiO_2/anthill clay as a heterogeneous catalyst for solar photocatalytic degradation of textile wastewater: catalyst characterization and optimization studies, Materialia, 8 (2019) 100484, doi: 10.1016/j.mtla.2019.100484.
[44] S. Danwittayakul, M. Jaisai, J. Dutta, Efficient solar photocatalytic degradation of textile wastewater using ZnO/ZTO composites, Appl. Catal., B, 163 (2015) 1–8.
[45] J.H. Shariffuddin, M.I. Jones, D.A. Patterson, Greener photocatalysts: hydroxyapatite derived from waste mussel shells for the photocatalytic degradation of a model azo dye wastewater, Chem. Eng. Res. Des., 91 (2013) 1693–1704.
[46] D. Gogoi, P. Makkar, R. Korde, M.R. Das, N.N. Ghosh, Exfoliated gC_3N_4 supported CdS nanorods as a S-scheme heterojunction photocatalyst for the degradation of various textile dyes, Adv. Powder Technol., 33 (2022) 103801, doi: 10.1016/j.apt.2022.103801.
[47] K. Ancy, M.R. Bindhu, J.S. Bai, M.K. Gatasheh, A.A. Hatamleh, S. Ilavenil, Photocatalytic degradation of organic synthetic dyes and textile dyeing waste water by Al and F co-doped TiO_2 nanoparticles, Environ. Res., 206 (2022) 112492, doi: 10.1016/j.envres.2021.112492.
[48] Md. Rashid Al-Mamun, Md. Shofikul Islam, Md. Rasel Hossain, S. Kader, Md. Shahinoor Islam, Md. Zaved Hossain Khan, A novel and highly efficient Ag and GO co-synthesized ZnO nano photocatalyst for Methylene blue dye degradation under UV irradiation, Environ. Nanotechnol. Monit. Manage., 16 (2021) 100495, doi: 10.1016/j.enmm.2021.100495.